Chemical Science

ROYAL SOCIETY OF CHEMISTRY

EDGE ARTICLE

View Article Online
View Journal

Cite this: DOI: 10.1039/d5sc08209a

All publication charges for this article have been paid for by the Royal Society of Chemistry

Rh(III)-catalyzed heteroannular-selective heteroarylation of biaryls: facile access to heteroacenes with sulfur-embedded 5–7 ring topology

Zhanhui He,[a] Li Yang,[a] Menghang Zhou,[a] Yue Zhong,[a] Zheng Liu,[ab]* Ziao Zhang,[a] Feiyang Xia,[a] Xuezhe Deng,[a] Shuang Yan,[b] Cheng Xu,[a] Cheng Zhang[c]* and Guodong Yin[a]*

Received 23rd October 2025
Accepted 2nd January 2026

DOI: 10.1039/d5sc08209a

rsc.li/chemical-science

Acenes with non-benzenoid 5–7 ring topology have drawn significant attention. Nevertheless, introducing sulfur atoms into 5/7-membered rings of acenes has not yet been achieved owing to synthetic challenges. Disclosed herein is a rhodium-catalyzed heteroannular-selective C–H/C–H oxidative cross-coupling reaction of 2-substituted biaryls with heteroarenes, which provides a convenient approach to heteroacenes with sulfur-embedded 5–7 ring topology. This protocol demonstrates excellent regioselectivity and broad functional group tolerance, enabling the efficient synthesis of a diverse library of thioether- and seleno-ether-substituted biheteroaryl compounds. Heteroacenes featuring sulfur-embedded 5–7 or 5–6 ring topologies can be switchably constructed through further intramolecular cyclization involving directing groups. Crystal structure analysis, along with studies on photophysical properties and aromaticity, indicates that heteroacenes with sulfur-embedded 5–7 ring topology have the potential as high-performance organic semiconductor materials.

Introduction

Acenes, characterized by linearly arranged benzenoid units, have attracted significant attention in the field of organic field-effect transistors (OFETs) due to their remarkable charge transport performance.[1] Nevertheless, larger acenes suffer from high sensitivity to oxidation by O_2 and readily undergo dimerization *via* formal [4 + 4] cycloaddition reactions, severely limiting their applications as organic functional materials.[2] The introduction of non-benzenoid five- and seven-membered ring arrays has emerged as a pivotal strategy to modulate the stability and optoelectronic properties of acenes (Scheme 1a).[3] In 2022, Jiang, Chi, and co-workers reported azulene-fused acenes with a 6–5–7 ring topology, demonstrating enhanced chemical stability compared to corresponding acenes.[4] Concurrently, acenes fused with azulene in a 6–7–5 ring configuration display anti-Kasha emission (even with double anti-Kasha bands) and function as hole-transporting semiconductors.[5] The integration of 5–7 ring pairs into heteroacene frameworks has also been explored.[6] For example, Gao, Swager *et al.* successfully synthesized *N*-doped heptacene incorporating azulene units, which demonstrated exceptional electronic transport properties.[7] Additionally, sulfur-bridged azulene-based acene forms charge-segregated assembly in the crystalline state, achieving a high charge-carrier mobility of 1.7 $cm^2 V^{-1} s^{-1}$.[8] Notably, the incorporation of diverse heteroatoms not only tunes the electronic properties and intermolecular interactions of acenes, but also significantly influences the optoelectronic performance of organic functional materials.[9] To date, the development of novel heteroacenes through embedding heteroatoms into 5–7 ring pairs remains highly desirable.[10]

As an isoelectronic counterpart of benzene, thiophene exhibits good planarity and aromaticity. Thiophene-fused materials not only demonstrate enhanced antioxidative stability,[11] but also enable the formation of intermolecular S···S, S···H, and S···π interactions.[12] These noncovalent interactions facilitate efficient charge transport and may significantly influence molecular packing arrangements. Therefore, thiophene-fused acenes exhibit excellent OFET performance,[13] and the maximum mobility of thin-film OFETs based on DPh-BTBT featuring five- and five-membered ring arrays reaches 2.0 $cm^2 V^{-1} s^{-1}$ (Scheme 1b).[14] Despite the disruption of the aromaticity of planar six-membered thiopyran,[15] thiophene- and thiopyran-fused polycyclic aromatics with five- and six-membered ring

[a]*Hubei Key Laboratory of Pollutant Analysis and Reuse Technology, College of Chemistry and Chemical Engineering, Hubei Normal University, Huangshi 435002, P. R. China. E-mail: zhengliu0827@hbnu.edu.cn; gdyin@hbnu.edu.cn*

[b]*Medical Imaging Key Laboratory of Sichuan Province, North Sichuan Medical College, Nanchong 637000, P. R. China*

[c]*Key Laboratory of Green Chemistry and Technology of Ministry of Education, College of Chemistry, Sichuan University, 29 Wangjiang Road, Chengdu 610064, P. R. China. E-mail: cheng.zhang@scu.edu.cn*

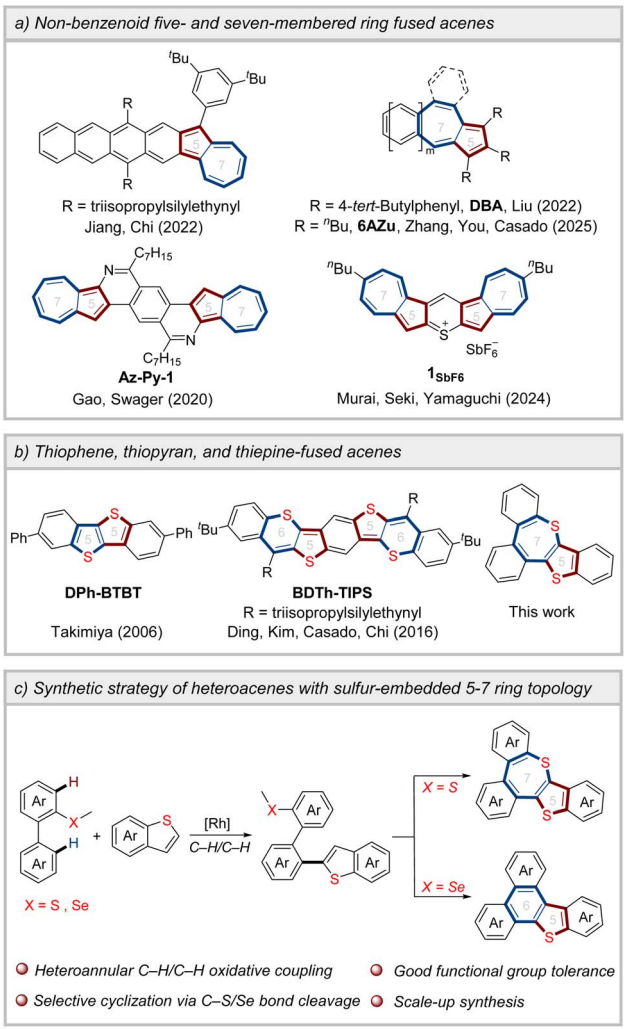

Scheme 1 Design and synthetic strategy of heteroacenes with sulfur-embedded 5–7 ring topology.

structures have drawn considerable attention.[16] In contrast, thiepine-based skeletons incorporating a sulfur-containing seven-membered ring have rarely been reported, primarily owing to synthetic challenges.[17]

C–H activation has emerged as a powerful strategy for constructing π-conjugated structures,[18] especially through C–H arylation/cyclization approaches, which significantly simplify synthetic pathways.[19] We envisioned that the heteroannular-selective heteroarylation of biaryls, followed by directing group-participated intramolecular cyclization, could serve as an effective strategy for constructing sulfur-embedded heteroacenes (Scheme 1c). Nevertheless, achieving the C–H/C–H oxidative coupling reaction of biaryls remains a challenge due to poor regioselectivity, as chelation-assisted transition metal-catalyzed C–H bond activation predominantly occurs at the *ortho*-position of the directing groups.[20] When employing a thioether as the directing group, the transition metal coordinates with the sulfur atom and activates the heteroannular C–H bond of the biaryl, leading to the formation of a six-membered cyclometalated intermediate.[21] This intermediate has lower ring strain compared to the four-membered cyclometalated intermediate generated by activating the *ortho*-C–H bond, thus enabling regioselectivity.[22] Herein, we present the heteroannular-selective heteroarylation of biaryls for constructing thiophene- and thiepine-fused polycyclic aromatics. Crystal structure analysis and DFT calculations indicate that heteroacenes with sulfur-embedded 5–7 ring topology have the potential as high-performance organic semiconductor materials.

Results and discussion

The initial investigation into the oxidative heteroannular-selective cross-coupling reaction was carried out using (3′-(*tert*-butyl)-[1,1′-biphenyl]-2-yl)(methyl)sulfane (**1a**) and benzo[*b*]thiophene (**2a**) as model substrates under the catalytic system of $[Cp^*RhCl_2]_2$/$AgSbF_6$. To our delight, when Ag_2O was used as an oxidant, and pivalic acid (PivOH) as an additive in tetrahydrofuran (THF), the desired product **3a** was obtained in 35% yield (Table S1, entry 1). The solvent screening indicated that DCE could enhance the yield of **3a** to 41% (Table S1). The catalysts of Pd(II), Ir(III), and Rh(III) could all promote the coupling reaction. Notably, $Cp^*Rh(MeCN)_3[SbF_6]_2$ demonstrated superior catalytic performance (Table S2). Further optimization of the oxidant revealed that Ag_2O was a more appropriate choice, and other oxidants, such as Ag_2CO_3, AgOAc, and AgF, exhibited lower efficiency than Ag_2O (Table S3). Additionally, it was found that the addition of bases had an inhibitory influence on the reaction, while acid additives could promote the formation of **3a** (Table S4). Attempts to decrease the amount of **2a** were unsuccessful, as the heteroarene decomposed under the reaction conditions (Table S5, entries 7 and 8). Further reduction of the oxidant Ag_2O loading to 3.0 equivalents resulted in a lower yield of 71% (Table S5, entry 9). Finally, **3a** was synthesized with a yield of 76% by employing $Cp^*Rh(MeCN)_3[SbF_6]_2$ as a catalyst, Ag_2O as an oxidant, and PivOH as an additive in DCE at 120 °C for 24 h (Table S5, entry 2).

With the optimized conditions established, a systematic exploration of the scope of heteroarenes (**2**) was conducted using **1a** as the coupling reagent (Scheme 2). The 3-, 4-, and 6-substituted benzo[*b*]thiophenes gave rise to the coupling products with yields ranging from 40% to 83% (**3b–3e**). When thiophenes were employed as the heteroarylation reagent, the cross-coupling reaction proceeded smoothly, affording the corresponding products in 33–74% yields (**3f–3o**). This catalytic system exhibited excellent tolerance towards thiophenes bearing electron-donating groups (–Me, –^{n}Bu, and –Ph) and electron-withdrawing groups (–CHO and –COOMe) at the C2 position (**3h–3l**, 52–74%). Furthermore, several disubstituted thiophenes were also identified as suitable substrates for this reaction (**3m–3o**, 52–73%). Additionally, thieno[3,2-*b*]thiophene (**2p**) and *N*-methylindole (**2q**) were demonstrated to be compatible with the catalytic system. Nevertheless, the yields of the resultant products **3p** and **3q** were relatively low, attaining values of 44% and 36%, respectively.

Subsequently, the substrate scope was extended to 2-thioether-substituted biphenyls. The steric hindrance caused by the enlarged directing group (–S^{i}Pr) led to relatively low coupling efficiency (**4a**, 37%). Functional groups (–Me, –F, –Cl, –

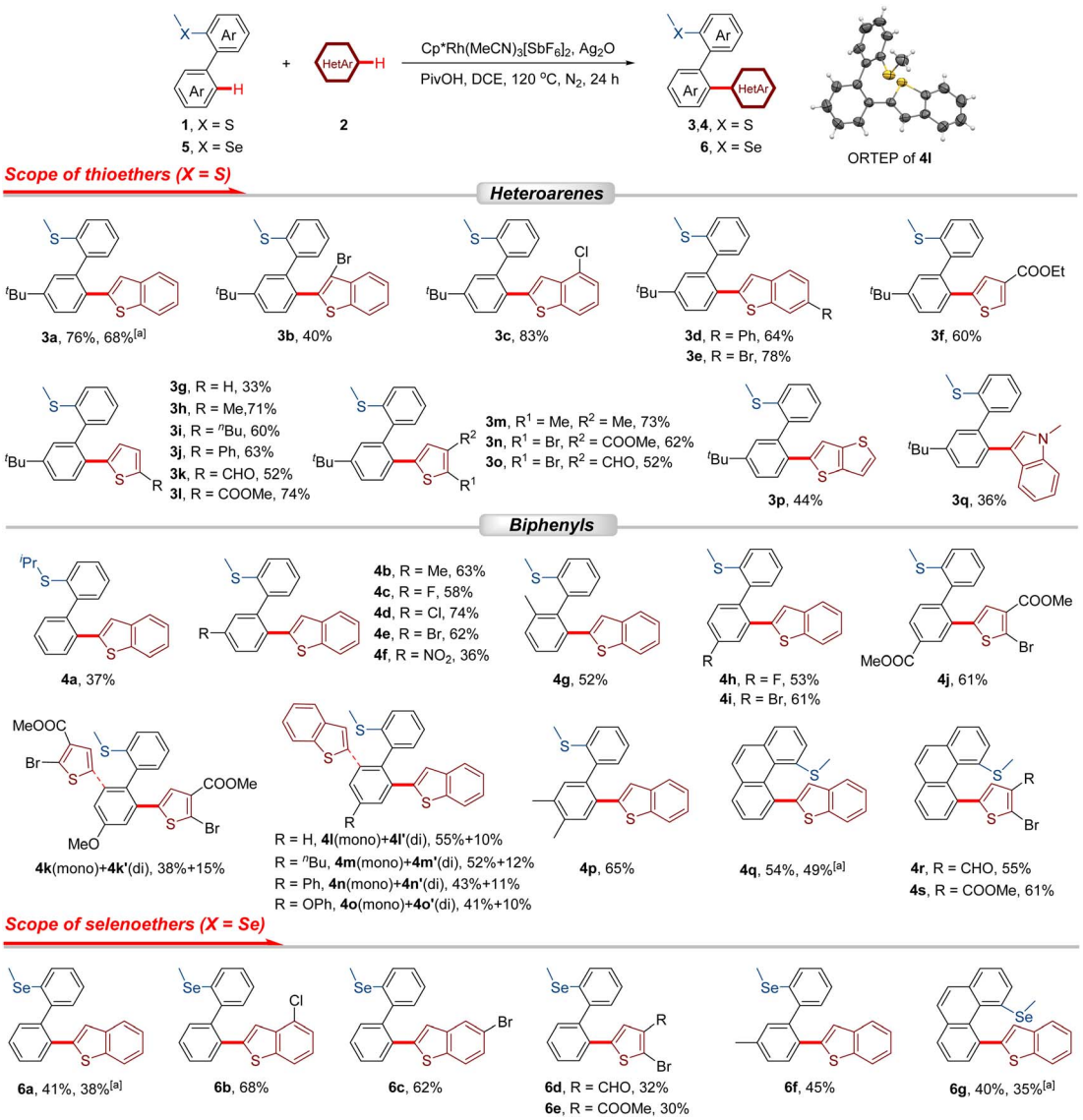

Scheme 2 Scope of substrates. Reaction conditions: **1** or **5** (0.2 mmol), **2** (0.6 mmol), $Cp^*Rh(MeCN)_3[SbF_6]_2$ (3 mol%), Ag_2O (0.7 mmol), PivOH (0.4 mmol) and DCE (1.0 mL) at 120 °C for 24 h under N_2. Isolated yields. [a]2.0 mmol scale.

Br, and $-NO_2$) substituted at the *meta*-position of [1,1′-biphenyl]-2-yl(methyl)sulfane can be well tolerated (**4b–4f**, 36–74%). The substrate with a methyl group at the *ortho*-position afforded heteroarylation product (**4g**) with a yield of 52%. The cross-coupling could also work well with *para*-substituted 2-thioether biphenyls (**4h–4k**, **4m–4o**). For unsubstituted biaryls or those bearing *para*-electron-donating groups, both mono- and di-heteroarylated products were obtained (**4k–4o**, **4k′–4o′**), whereas substrates featuring *para*-electron-withdrawing substituents exclusively afforded the mono-heteroarylated derivatives (**4h–4j**), with only trace amounts of the corresponding di-heteroarylated species observed. Notably, in the catalytic systems involving *ortho*- and *meta*-substituted biaryl substrates, no di-heteroarylated products were detected, which can be attributed to steric hindrance. The structure of product **4l** was further confirmed by X-ray crystallography. (3′,4′-Dimethyl-[1,1′-biphenyl]-2-yl)(methyl)sulfane and methyl(phenanthren-4-yl)sulfane could undergo the oxidative coupling reactions in moderate yields (**4p–4s**, 54–65%).

As a member of the same group as the sulfur atom, the selenium atom could also serve as a directing group to facilitate the selective heteroannular C–H bond activation of biphenyls, thereby enriching the diversity of products. A series of selenoether-substituted biheteroaryls were successfully synthesized under the rhodium catalytic system (**6a–6g**, 30–68%).

The scale-up synthesis of compounds **3a**, **4q**, **6a**, and **6g** was successfully accomplished on a 2.0 mmol scale, paving the way for the further development and construction of heteroacenes (Scheme S4). In addition, the oxidant Ag_2O could be regenerated through treatment with HNO_3 and NaOH. When the regenerated Ag_2O was reused as the oxidant, the performance of the oxidative coupling reaction remained unaffected (Scheme S5).

To delve deeper into the heteroannular-selective oxidative cross-coupling, the H/D exchange experiments were performed (Scheme 3a). In the absence and presence of **2a**, 12% and 10% deuterium rates of C2′–H of biphenyl in **1m** were observed, respectively, indicating the reversible process of the heteroannular C–H metalation (Schemes S6 and S8). Furthermore, the reaction of **2a** with D_2O resulted in 24% and 20% deuterium rates of C2–H of **2a** in the absence and presence of **1m**, respectively, demonstrating that the cleavage of C2–H of **2a** is reversible (Schemes S7 and S8). Kinetic isotope effect (KIE) experiments were conducted for **1m** and **2a**. A KIE value of 1.29 was observed in the parallel reactions of **1m** and [D_5]-**1m** with **2a**, while a KIE value of 0.96 was detected in the parallel reactions between **2a** and [D]-**2a** with **1m**. These results suggest that the C–H cleavage of **1m** and **2a** may not be involved in the rate-determining step (Tables S6 and S7).

The plausible mechanistic pathway was proposed (Scheme 3b). The coordination of **1m** to Rh(III), followed by heteroannular C–H activation, leads to the formation of a six-membered cyclometalated complex **IM1**. Subsequently, the second C–H activation on **2a** delivers intermediate **IM2**. The reductive elimination of **IM2** gives product **4l** and Rh(I), which is then oxidized by Ag(I) and re-enters the catalytic cycle.

Following the preparation of the coupling products, the intramolecular cyclization reaction was carried out to construct the sulfur-embedded polycyclic aromatics. Under the oxidation/cyclization reaction conditions, compounds **7a** and **7b** were successfully synthesized, with yields of 69% and 34%, respectively, *via* the cleavage of the C sp^3–S bond (Scheme 4a). Intriguingly, under identical experimental conditions, the selenomethyl-substituted biheteroaryls (**6a** and **6g**) underwent cleavage of the C sp^2–Se bond, leading to the formation of the six-membered ring products **8a** and **8b** (Scheme 4b). Moreover, by adjusting the equivalents of the oxidant, it was feasible to achieve the selective oxidation of **7a**, thereby obtaining compounds **9** and **10** (Scheme 4c).

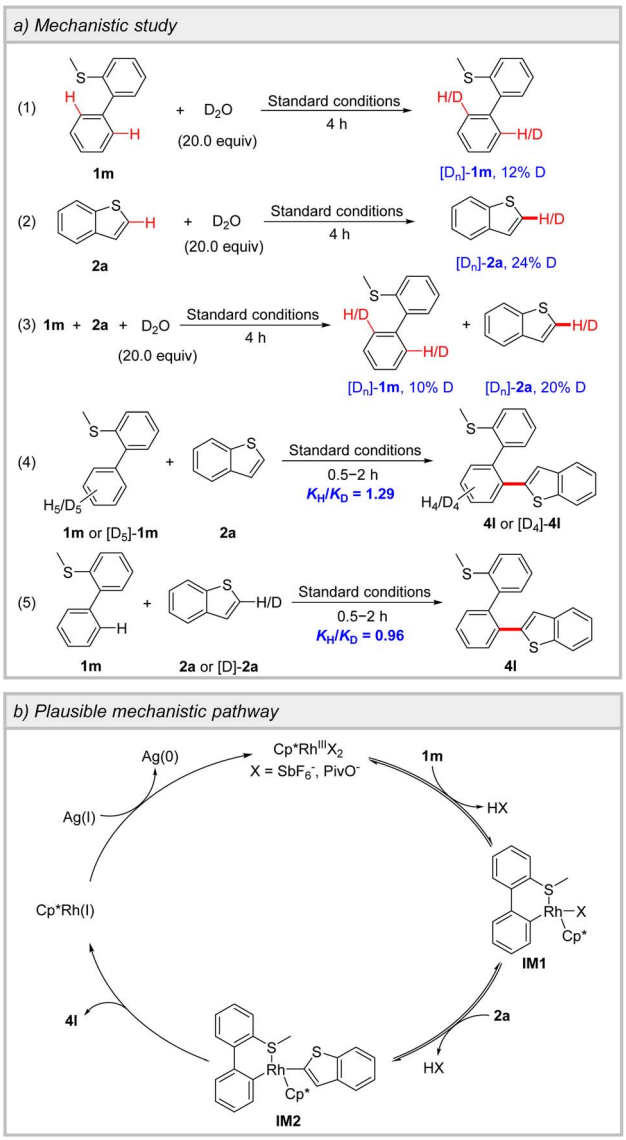

Scheme 3 Mechanistic study and plausible mechanistic pathway.

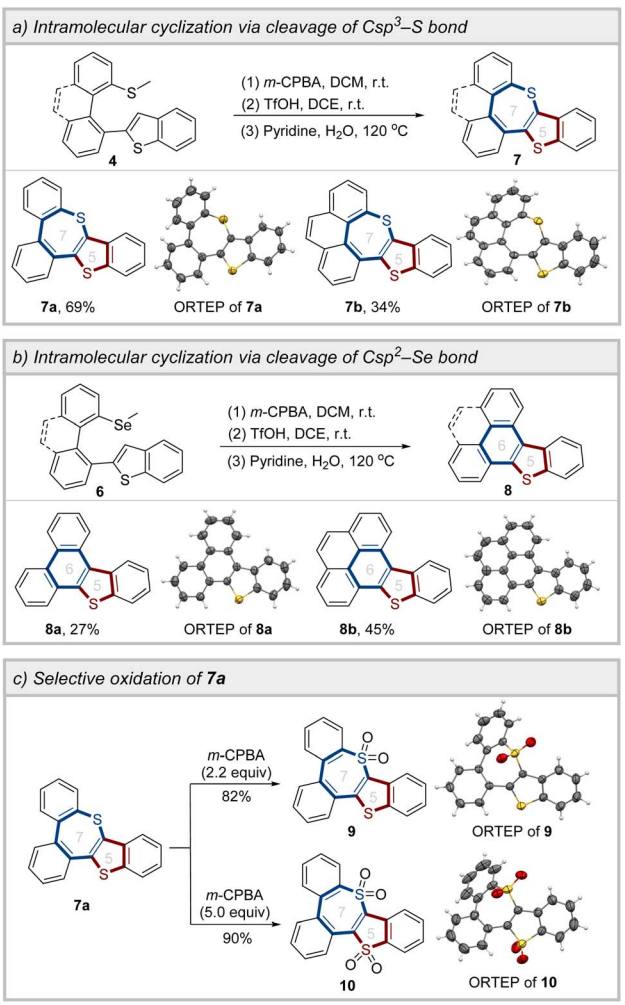

Scheme 4 Synthetic applications.

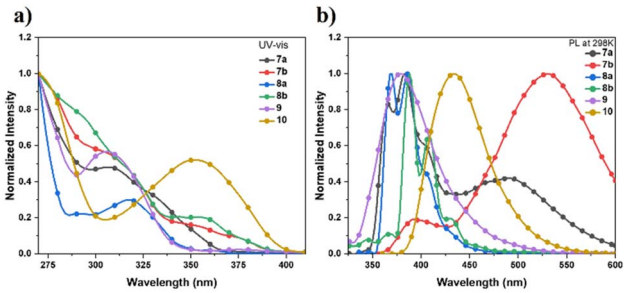

Fig. 1 (a) Absorption spectra and (b) fluorescence emission spectra of **7a**, **7b**, **8a**, **8b**, **9**, and **10** in CH_2Cl_2 (1.0×10^{-5} M).

The UV-vis absorption and fluorescence emission spectra of these sulfur-embedded polycyclic aromatics in diluted CH_2Cl_2 (1.0×10^{-5} mol L^{-1}) were measured (Fig. 1, S1 and Table S8). The absorption maxima of compounds **7a**, **7b**, **8a**, and **8b** are observed at 306, 304, 318, and 354 nm, respectively. Compared with **7a**, the oxidation of the sulfur atoms to sulfone groups in compound **10** results in a bathochromically shifted absorption peak from 306 nm to 354 nm. According to the time dependent density functional theory (TD-DFT) calculations (Tables S9–S14), the absorption maxima of **7a** and **9** were assigned to the $S_0 \rightarrow S_2$ excitation, the shoulder peak of **7b** between 310–380 nm were ascribed to the transitions of S_0 to S_n (n = 1–4). Compounds **7a** and **7b** exhibit photoluminescence peaks at 360, 384, 500 nm and 392, 532 nm, respectively. The bathochromic-shifted emission band of **7b** can be attributed to the extension of π-conjugation. In contrast, compounds **8a**, **8b**, **9**, and **10** display relatively blue-shifted emission bands.

Single crystals of these sulfur-embedded polycyclic aromatics were obtained *via* the solvent diffusion method with dichloromethane and hexane. The crystal structures and packing modes of these six single crystals are shown in Fig. 2 and S2–S8. Moreover, detailed crystallographic data are summarized in Tables S16–S21. Owing to the existence of the sulfur-containing seven-membered ring, compound **7a** presents a V-shaped geometry rather than a plane one. A C–S–C bond angle of 70.7° is observed, and the dihedral angle between the benzene ring and the thiophene ring is measured to be 43.4°. The distance between the S atoms is 3.38 Å, indicating the existence of S···S interactions among molecules. In the π-extended **7b**, the C–S–C bond angle decreases to 55.8°. Moreover, a twist angle of 8.6° is observed for the phenanthrene ring. **7b** exhibits 2D "brick-wall" lamellar stacking arrangement, and the π–π stacking distances are 3.40 and 3.43 Å. Compounds **8a** and **8b**, featuring planar geometry, display herringbone packing. Notably, **8b** exhibits a smaller π–π overlap than **7b**, whose crystal packing mode is influenced by the seven-membered ring (Fig. 2e and f). As a common approach for regulating the intermolecular interactions, the formation of intermolecular C–H···O hydrogen bonds were accomplished by oxidizing the sulfur atoms to sulfone groups.

To gain insights into the aromaticity, the Harmonic oscillator model of aromaticity (HOMA) values and anisotropy of the induced current density (ACID) were calculated (Fig. 3 and 4). The benzene rings and the five-membered sulfur-containing thiophene rings in compounds **7a**, **7b**, **8a**, **8b**, **9**, and **10** display positive HOMA values, thereby indicating their aromatic properties. Meanwhile, the chalcogen-containing seven-membered rings in **7a** and **7b** possess relatively small positive HOMA values of 0.09 and 0.14, respectively, suggesting weak aromatic characteristics. Upon the oxidation of the sulfur atom within the seven-membered ring to a sulfone group, the aromaticity of thiepine is enhanced. Conversely, when the sulfur atom in the five-membered ring is oxidized to sulfone, the aromaticity of thiophene diminishes. ACID plots of **8a** and **8b** show a clockwise ring current along the periphery of the whole backbone, indicating the global aromatic characteristics, while weaker diatropic ring current were observed on sulfur-embedded seven-membered rings of **7a**, **7b**, **9**, and **10**.

The HOMOs and the LUMOs of these sulfur-embedded polycyclic aromatics are shown in Tables S22 and S23. Compounds **8a** and **8b** exhibit narrower bandgaps compared to **7a** and **7b**, respectively, consistent with the results of photophysical measurements. This can be attributed to the disruption of conjugation caused by the sulfur-containing seven-membered ring. The introduction of sulfone results in deeper LUMOs of −1.71 eV (**9**) and −2.62 eV (**10**). The electrostatic

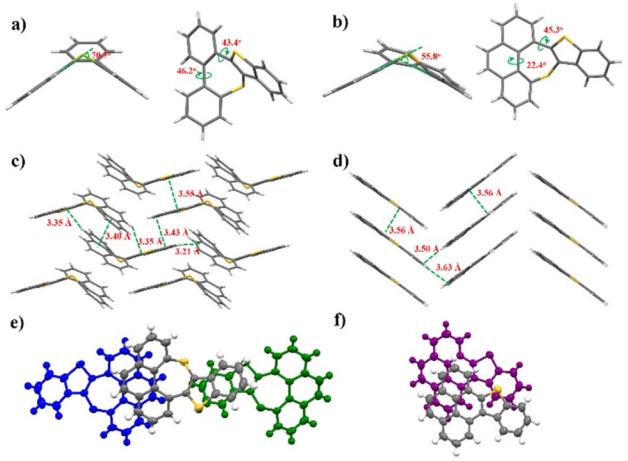

Fig. 2 X-ray single-crystal structures of (a) **7a**, and (b) **7b**; crystal packings of (c) **7b**, and (d) **8b**; π-stacked molecules of (e) **7b**, and (f) **8b**.

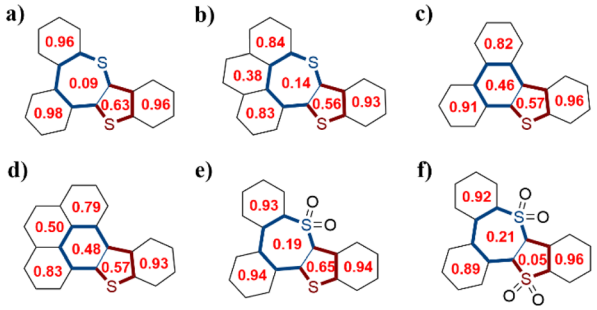

Fig. 3 The calculated HOMA values of (a) **7a**, (b) **7b**, (c) **8a**, (d) **8b**, (e) **9**, and (f) **10**.

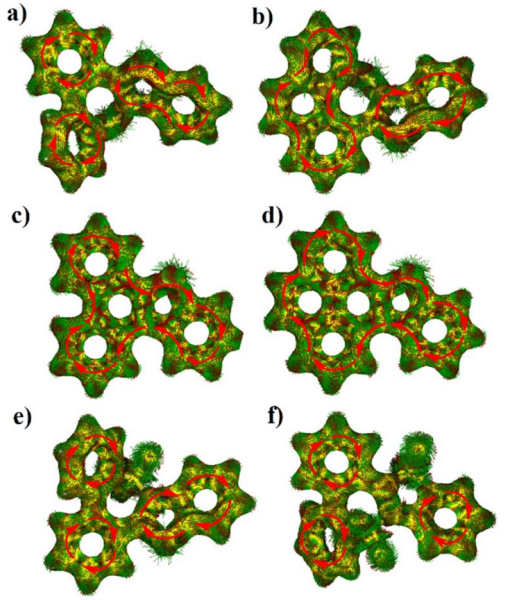

Fig. 4 Calculated ACID plots of (a) **7a**, (b) **7b**, (c) **8a**, (d) **8b**, (e) **9**, and (f) **10**. The red arrows indicate the ring current flow.

potential maps are presented in Fig. S9. For compounds **7a** and **7b**, the electron density is concentrated on the sulfur-containing seven-membered rings. In contrast, compounds **8a** and **8b** show a more delocalized electron distribution across the conjugated framework. When the sulfur atoms are oxidized to sulfone groups, the π-cores of compounds **9** and **10** exhibit electron deficiency. The electron density is predominantly concentrated on the oxygen atoms, suggesting that these compounds are more prone to form intermolecular C–H···O hydrogen bonds.

Hirshfeld surface analysis was performed to quantitatively analyze the intermolecular interactions (Fig. S10–S12). The S···S interaction (2.4%) in **7a** demonstrates the influence of the introduction of the sulfur-containing seven-membered ring on intermolecular interactions. The ratio of π–π interactions (C···C) of **7b** (15.1%) and **8b** (14.2%) is higher than that of **7a** (5.0%) and **8a** (11.3%), which can be attributed to the extended π-plane. The oxidation of sulfur atoms led to O···H interactions of **9** (18.4%) and **10** (36.2%), which are consistent with the results from the crystal structure analysis.

Conclusions

In summary, the incorporation of sulfur-containing 5–7 ring topology into acenes has been successfully achieved *via* heteroannular-selective C–H/C–H oxidative cross-coupling of 2-substituted biaryls with heteroarenes followed by directing group-involved intramolecular cyclization. A diverse library of thioether- and selenoether-substituted biheteroaryl compounds can be efficiently synthesized, owing to the excellent regioselectivity and high functional group tolerance of this protocol. Under oxidation/cyclization conditions, the cleavage of the C sp^3–S bond of biheteroaryl compounds delivers thiophene- and thiepine-fused polycyclic aromatics **7**, while the cleavage of the C sp^2–Se bond generates thiophene and benzene rings fused products **8**. Although the introduction of the seven-membered thiepine ring compromises molecular planarity and aromaticity, the crystal structure of **7b** exhibits a "brick-wall" lamellar stacking arrangement, whereas compound **8a**, which possesses a planar geometry, adopts a herringbone packing motif. The selective oxidation of sulfur atoms from **7a** to **9** and **10**, achieved by adjusting the equivalents of the oxidant, reduces the electron density of the molecular framework and enables the formation of intermolecular C–H···O hydrogen bonds. Crystal structure analysis and DFT calculations indicate that heteroacenes with sulfur-embedded 5–7 ring topology have the potential as high-performance organic semiconductor materials.

Author contributions

Z. L., C. Z., and G. Y. conceived and supervised the project. Z. H. and L. Y. designed and carried out the experiments, analyzed the data, and wrote the manuscript. M. Z., Y. Z., Z. Z., F. X., and X. D. provided valuable assistance with the synthesis of compounds. S. Y. and C. X. contributed to experimental testing and analysis. All authors discussed the results and commented on the manuscript.

Conflicts of interest

There are no conflicts to declare.

Data availability

CCDC 2281727 (**4l**), 2433068 (**7a**), 2475673 (**7b**), 2433061 (**8a**), 2433067 (**8b**), 2433062 (**9**) and 2433063 (**10**) contain the supplementary crystallographic data for this paper.[23a–g]

The data supporting this article have been included as part of the supplementary information (SI). Supplementary information: further information, including general experimental information, optimization studies, detailed experimental procedures, compound characterization data and NMR spectra of new compounds. See DOI: https://doi.org/10.1039/d5sc08209a.

Acknowledgements

Financial support from the National Natural Science Foundation of China (No. 22301071), the Special Fund Project for Guiding Local Science and Technology Development of Hubei Province by the Central Government (No. 2024CSA097), Natural Science Foundation of Hubei Province (No. 2023AFB459), Excellent Young and Middle-aged Science and Technology Innovation Team Program of Universities in Hubei Province (No. T2024014), Opening Project of Medical Imaging Key Laboratory of Sichuan Province (No. MIKL202406), Open Research Fund of Hubei Key Laboratory of Pollutant Analysis & Reuse Technology (No. PA220204), and Hubei Normal University 2023 Talent Introduction Project (HS2023RC064).

Notes and references

1 (*a*) J. E. Anthony, *Angew. Chem., Int. Ed.*, 2008, **47**, 452–483; (*b*) A. N. Lakshminarayana, A. Ong and C. Chi, *J. Mater. Chem. C*, 2018, **6**, 3551–3563; (*c*) W. Chen, F. Yu, Q. Xu, G. Zhou and Q. Zhang, *Adv. Sci.*, 2020, **7**, 1903766; (*d*) H. Hayashi and H. Yamada, *Chem. Sci.*, 2025, **16**, 11204–11231.

2 (*a*) X. Shi and C. Chi, *Chem. Rec.*, 2016, **16**, 1690–1700; (*b*) S. S. Zade, N. Zamoshchik, A. R. Reddy, G. Fridman-Marueli, D. Sheberla and M. Bendikov, *J. Am. Chem. Soc.*, 2011, **133**, 10803–10816.

3 (*a*) J. Guo, F. Du, B. Yu, P. Du, H. Li, J. Zhang and H. Xin, *Chem. Sci.*, 2024, **15**, 12589–12597; (*b*) Y. He, Y. Zhu, M. Luo and H. Xia, *Chin. Chem. Lett.*, 2025, **36**, 110463.

4 A. Ong, T. Tao, Q. Jiang, Y. Han, Y. Ou, K.-W. Huang and C. Chi, *Angew. Chem., Int. Ed.*, 2022, **61**, e202209286.

5 (*a*) S. Wang, M. Tang, L. Wu, L. Bian, L. Jiang, J. Liu, Z.-B. Tang, Y. Liang and Z. Liu, *Angew. Chem., Int. Ed.*, 2022, **61**, e202205658; (*b*) F. Huang, M. Díaz-Fernández, J. M. Marín-Beloqui, L. Sun, Y. Chen, S. Liu, Y. Wang, H. Zheng, S. Li, C. Zhang, J. You and J. Casado, *J. Am. Chem. Soc.*, 2025, **147**, 1574–1583.

6 (*a*) M. Murai, M. Abe, S. Ogi and S. Yamaguchi, *J. Am. Chem. Soc.*, 2022, **144**, 20385–20393; (*b*) H. Xin, J. Li, X. Yang and X. Gao, *J. Org. Chem.*, 2020, **85**, 70–78; (*c*) C. Duan, J. Zhang, S. Cai, J. Xiang, X. Yang and X. Gao, *Eur. J. Org Chem.*, 2023, **26**, e202201347.

7 H. Xin, J. Li, R.-Q. Lu, X. Gao and T. M. Swager, *J. Am. Chem. Soc.*, 2020, **142**, 13598–13605.

8 S. Takahashi, M. Murai, Y. Hattori, S. Seki, T. Yanai and S. Yamaguchi, *J. Am. Chem. Soc.*, 2024, **146**, 22642–22649.

9 (*a*) J. Freudenberg and U. H. F. Bunz, *J. Am. Chem. Soc.*, 2024, **146**, 16937–16949; (*b*) U. H. F. Bunz and J. Freudenberg, *Acc. Chem. Res.*, 2019, **52**, 1575–1587; (*c*) Y. Guo, C. Chen and X.-Y. Wang, *Chin. J. Chem.*, 2023, **41**, 1355–1373.

10 H. Luo and J. Liu, *Angew. Chem., Int. Ed.*, 2023, **62**, e202302761.

11 J. G. Laquindanum, H. E. Katz and A. J. Lovinger, *J. Am. Chem. Soc.*, 1998, **120**, 664–672.

12 (*a*) M. D. Curtis, J. Cao and J. W. Kampf, *J. Am. Chem. Soc.*, 2004, **126**, 4318–4328; (*b*) C. Wang, H. Dong, W. Hu, Y. Liu and D. Zhu, *Chem. Rev.*, 2012, **112**, 2208–2267.

13 (*a*) C. Wang, D. Hashizume, M. Nakano, T. Ogaki, H. Takenaka, K. Kawabata and K. Takimiya, *Chem. Sci.*, 2020, **11**, 1573–1580; (*b*) T. Okamoto, C. P. Yu, C. Mitsui, M. Yamagishi, H. Ishii and J. Takeya, *J. Am. Chem. Soc.*, 2020, **142**, 9083–9096; (*c*) H. Jiang, S. Zhu, Z. Cui, Z. Li, Y. Liang, J. Zhu, P. Hu, H.-L. Zhang and W. Hu, *Chem. Soc. Rev.*, 2022, **51**, 3071–3122; (*d*) Y. Zhang, Y. Wang, C. Gao, Z. Ni, X. Zhang, W. Hu and H. Dong, *Chem. Soc. Rev.*, 2023, **52**, 1331–1381; (*e*) Y. Chen, Z. Wu, Z. Chen, S. Zhang, W. Li, Y. Zhao, Y. Wang and Y. Liu, *Chem. Sci.*, 2024, **15**, 11761–11774.

14 K. Takimiya, H. Ebata, K. Sakamoto, T. Izawa, T. Otsubo and Y. Kunugi, *J. Am. Chem. Soc.*, 2006, **128**, 12604–12605.

15 (*a*) S. Dong, T. Seng Herng, T. Y. Gopalakrishna, H. Phan, Z. L. Lim, P. Hu, R. D. Webster, J. Ding and C. Chi, *Angew. Chem., Int. Ed.*, 2016, **55**, 9316–9320; (*b*) Y. Qiao, L. Yang, J. Zhu, C. Yan, D. Chang, N. Zhang, G. Zhou, Y. Zhao, X. Lu and Y. Liu, *J. Am. Chem. Soc.*, 2021, **143**, 11088–11101; (*c*) Z. Liu, W. Han, J. Lan, L. Sun, J. Tang, C. Zhang and J. You, *Angew. Chem., Int. Ed.*, 2023, **62**, e202211412; (*d*) W.-W. Yang, Z.-H. Ren, J. Feng, Z.-B. Lv, X. Cheng, J. Zhang, D. Du, C. Chi and J.-J. Shen, *Angew. Chem., Int. Ed.*, 2024, **63**, e202412681.

16 X. Shi, E. Quintero, S. Lee, L. Jing, T. Seng Herng, B. Zhang, K.-W. Huang, J. T. L. Navarrete, J. Ding, D. Kim, J. Casado and C. Chi, *Chem. Sci.*, 2016, **7**, 3036–3046.

17 (*a*) Z. Cai, H. Zhang, H. Geng, Z. Liu, S. Yang, H. Luo, L. Jiang, Q. Peng, G. Zhang, J. Chen, Y. Yi, W. Hu and D. Zhang, *Chem.–Eur. J.*, 2013, **19**, 14573–14580; (*b*) W. Wang, F. Hanindita, Y. Tanaka, K. Ochiai, H. Sato, Y. Li, T. Yasuda and S. Ito, *Angew. Chem., Int. Ed.*, 2023, **62**, e202218176.

18 (*a*) Y. Segawa, T. Maekawa and K. Itami, *Angew. Chem., Int. Ed.*, 2015, **54**, 66–81; (*b*) W. Hagui, H. Doucet and J.-F. Soulé, *Chem*, 2019, **5**, 2006–2078; (*c*) B. Li, A. I. M. Ali and H. Ge, *Chem*, 2020, **6**, 2591–2657; (*d*) I. A. Stepek and K. Itami, *ACS Mater. Lett.*, 2020, **2**, 951–974; (*e*) K. Wang, J. Zhang, R. Hu, C. Liu, T. A. Bartholome, H. Ge and B. Li, *ACS Catal.*, 2022, **12**, 2796–2820.

19 (*a*) Y. Yang and J. You, *Prog. Chem.*, 2020, **32**, 1824–1834; (*b*) Y. Yang, Y. Wu, Z. Bin, C. Zhang, G. Tan and J. You, *J. Am. Chem. Soc.*, 2024, **146**, 1224–1243.

20 (*a*) Z. Chen, B. Wang, J. Zhang, W. Yu, Z. Liu and Y. Zhang, *Org. Chem. Front.*, 2015, **2**, 1107–1295; (*b*) C. Liu, J. Yuan, M. Gao, S. Tang, W. Li, R. Shi and A. Lei, *Chem. Rev.*, 2015, **115**, 12138–12204; (*c*) Y. Yang, J. Lan and J. You, *Chem. Rev.*, 2017, **117**, 8787–8863; (*d*) C. Sambiagio, D. Schönbauer, R. Blieck, T. Dao-Huy, G. Pototschnig, P. Schaaf, T. Wiesinger, M. F. Zia, J. Wencel-Delord, T. Besset, B. U. W. Maes and M. Schnürch, *Chem. Soc. Rev.*, 2018, **47**, 6603–6743.

21 (*a*) G. Liao, T. Zhang, L. Jin, B.-J. Wang, C.-K. Xu, Y. Lan, Y. Zhao and B.-F. Shi, *Angew. Chem., Int. Ed.*, 2022, **61**, e202115221; (*b*) Y. Li, Y.-C. Liou, X. Chen and L. Ackermann, *Chem. Sci.*, 2022, **13**, 4088–4094; (*c*) J. Xu, W. Qiu, X. Zhang, Z. Wu, Z. Zheng, K. Yang and Q. Song, *Angew. Chem., Int. Ed.*, 2023, **62**, e202313388.

22 S. Yang, R. Cheng, M. Zhang, Z. Bin and J. You, *ACS Catal.*, 2019, **9**, 6188–6193.

23 (*a*) CCDC 2281727: Experimental Crystal Structure, 2026, DOI: 10.5517/ccdc.csd.cc2glb3j; (*b*) CCDC 2433068: Experimental Crystal Structure, 2026, DOI: 10.5517/ccdc.csd.cc2mnt26; (*c*) CCDC 2475673: Experimental Crystal Structure, 2026, DOI: 10.5517/ccdc.csd.cc2p34fd; (*d*) CCDC 2433061: Experimental Crystal Structure, 2026, DOI: 10.5517/ccdc.csd.cc2mnsvy; (*e*) CCDC 2433067: Experimental Crystal Structure, 2026, DOI: 10.5517/ccdc.csd.cc2mnt15; (*f*) CCDC 2433062: Experimental Crystal Structure, 2026, DOI: 10.5517/ccdc.csd.cc2mnswz; (*g*) CCDC 2433063: Experimental Crystal Structure, 2026, DOI: 10.5517/ccdc.csd.cc2mnsx0.